J Mol Model (2009) 15:1501–1507
DOI 10.1007/s00894-009-0502-5

ORIGINAL PAPER

Molecular dynamics simulations and MM–PBSA calculations of the lectin from snowdrop (*Galanthus nivalis*)

Zhen Liu · Yizheng Zhang

Received: 14 January 2009 / Accepted: 14 March 2009 / Published online: 17 May 2009

Abstract *Galanthus nivalis* agglutinin (GNA), a mannose-specific lectin from snowdrop bulbs, is a member of the monocot mannose-specific lectin family and exhibits antiviral activity toward HIV. In the present study, molecular dynamics (MD) simulations were performed to study the interaction between GNA and its carbohydrate ligand over a specific time span. By analysis of the secondary structures, it was observed that the GNA conformation maintains rather stable along the trajectories and the high fluctuations were only centered on the carbohydrate recognition domains. Our MD simulations also reproduced most of the hydrogen bonds observed in the x-ray crystal structure. Furthermore, the obtained MD trajectories were used to estimate the binding free energy of the complex using the molecular mechanics/Poisson Boltzmann surface area (MM-PBSA) method. It was revealed by the inspection of the binding free energy components that the major contributions to the complex stability arose from electrostatic interactions.

Keywords AMBER · *Galanthus nivalis* agglutinin (GNA) · Lectin · Molecular dynamics simulations (MD) · Molecular mechanics Poisson–Boltzmann surface area (MM-PBSA)

Electronic supplementary material The online version of this article (doi:10.1007/s00894-009-0502-5) contains supplementary material, which is available to authorized users.

Z. Liu · Y. Z. Zhang (✉)
Sichuan Key Laboratory of Molecular Biology and Biotechnology,
Key Laboratory of Bio-resources and Eco-environment,
Ministry of Education, College of Life Science,
Sichuan University,
Chengdu 610064, People's Republic of China
e-mail: yizzhang@scu.edu.cn

Z. Liu
e-mail: actg0101@gmail.com

Introduction

Lectins are oligomeric proteins with carbohydrate recognition functions which are widespread in plants. Advances in the structural analysis and molecular cloning of lectin genes enable subdivision of plant lectins in a limited number of subgroups of structurally and evolutionary related proteins. Four major lectin families, namely, the legume lectins, the chitin-binding lectins composed of hevein domains, the type 2 ribosome-inactivating proteins and the monocot mannose-binding lectins comprise the majority of all currently known plant lectins [1]. *Galanthus nivalis* agglutinin/lectin (GNA), a mannose-specific lectin from snowdrop bulbs (*Amaryllidaceae*), represents the super family of monocot mannose-specific lectins [2]. In contrast to other plant lectins, these lectins lack the ability to bind glucose and interact most specifically with high mannose glycoprotein that possess α-1, 3 andα-1, 6 linkages [3, 4].

GNA is a homotetramer composed of four identical noncovalently bound monomers of 109 residues (12 kDa) [5]. Its monomer consists of three pseudo-symmetrically related β-sheet domains, which are termed carbohydrate recognition domains (CRD1, CRD2, CRD3), each with a conserved mannose-binding site and corresponds to four-stranded β-sheets [5]. Crystal structures of the GNA have revealed that all 12 binding sites of the tetramer are functional (Fig. 1) [6].

The monomer of GNA complex with a branched mannopentaose ((Mana1,6-(a1,3-Man)Man-a1,6-(a1,3-Man)Man) is available in the protein data bank (PDB ID: 1JPC) [5]. The mannopentaose molecule binds in different binding modes at the highly occupied in CRD1 and the CRD3 binding sites. In both of these binding modes only the outer trimannoside branch is involved in

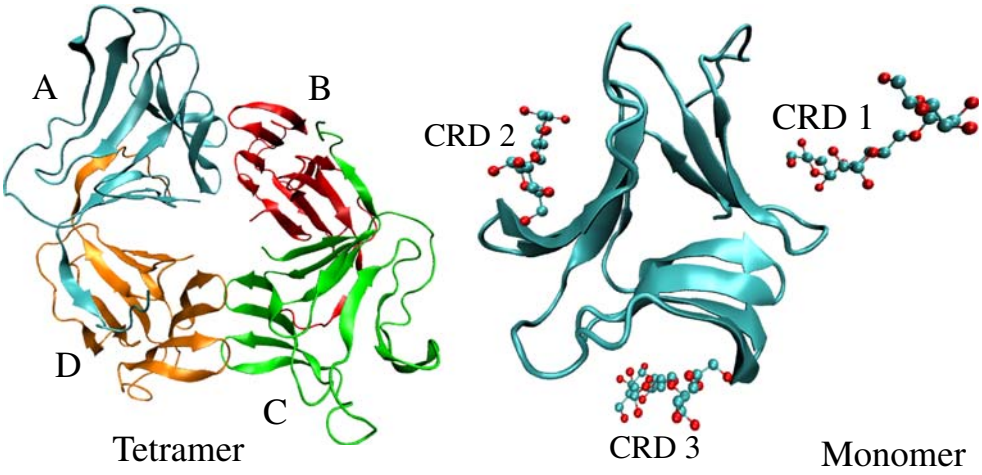

Fig. 1 Structure of GNA tetramer and monomer

binding interactions. In the CRD2 binding site, the observed electron density is weak and sufficient for fitting only two mannose residues (Fig. 1) [5, 7].

In the superfamily of monocot mannose-specific lectins, GNA was researched early and its anti-HIV activity mechanism was clearly represented [8, 9]. It is potent inhibitor of the HIV-induced cytopathicity and directly interfere with the virus-cell membrane fusion process by binding to the high-mannose glycans on gp120, the crucial envelope glycoprotein of HIV during the infection and blocking the binding of HIV to target cells [10]. A number of studies have clearly shown that the gp120 is extensively glycosylated, with N-linked complex and high mannose carbohydrates accounting for about half of the molecular weight [11, 12]. The binding of GNA to HIV is dependent on the high-mannose glycans on gp120.

A complete understanding of the molecular mechanisms determining the specific formation of complexes would be useful for the rational design of a protein. Molecular dynamics (MD) simulation can bring biomolecular structures alive, giving insights into the natural dynamics on different timescales in solution [13, 14]. Therefore, in the present paper, we focus on the interaction between the GNA and its mannoside ligands using MD simulation. Accurate analysis of the trajectory has yielded precious information about their interaction, and it might be very helpful for further development of GNA and other monocot mannose-binding lectins.

Methods and materials

Lectin structure preparation

The crystal structure of GNA (PDB ID: 1JPC) [5] was used as an initial structure for the MD simulations. Crystal water molecules were deleted before further processing. Two MD simulations were performed with and without ligand. In order to make a reliable comparison, the two systems were analyzed in the same way. The systems were solvated in a water box of 7689 TIP3P [15] water molecules using tLeap from the AMBER 9 [16] suite, leading to a periodic box size of approximately 65.419 Å×67.806 Å×72.229 Å. Three sodium ions were added to achieve neutrality of the systems.

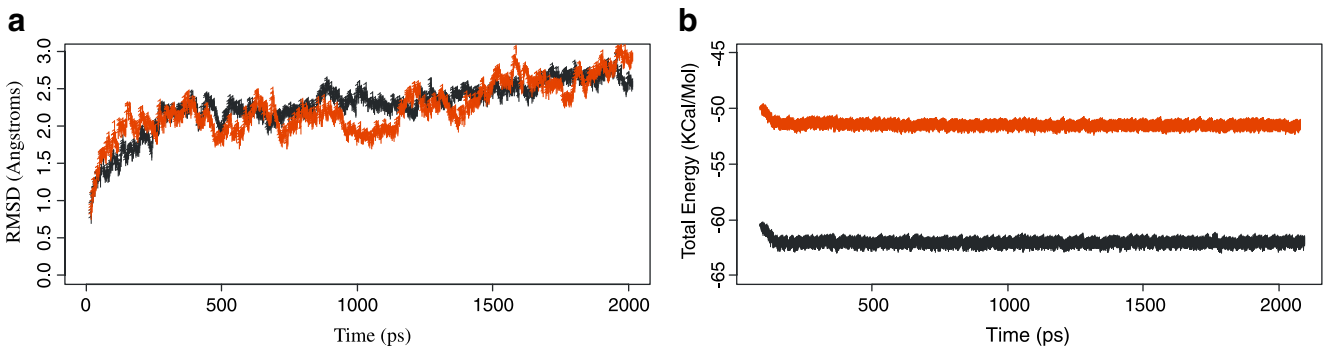

Fig. 2 (**a**) Root-mean-square deviations (Å) of GNA with (black line) and without ligand (red line) during 2000 ps MD simulations compared with the first coordinate frame. (**b**) Total energy fluctuations versus simulation time for GNA with (black line) and without ligand (red line)

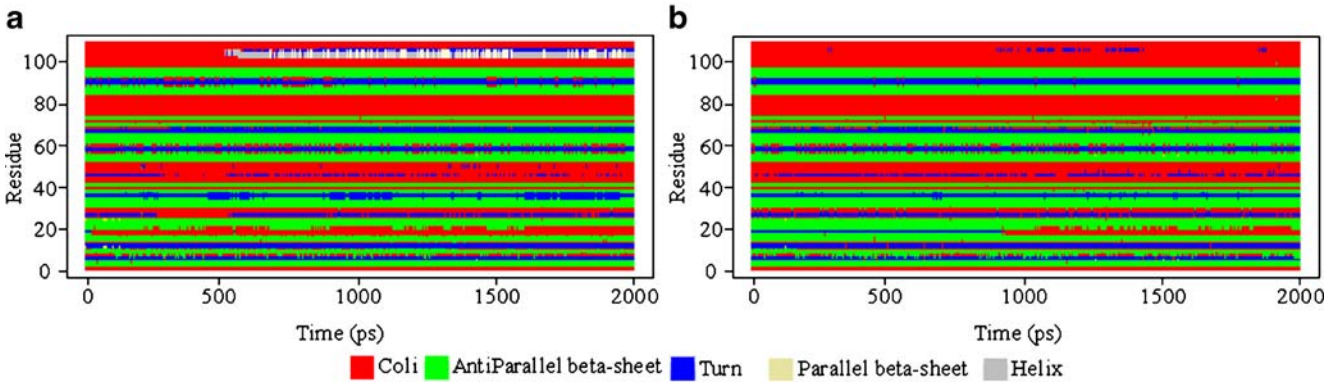

Fig. 3 Variation of the secondary structure for each residue along the complete trajectory (2000 ps). (**a**) ligand-bound; (**b**) ligand-free

Energy optimization and molecular dynamics

Energy minimization and molecular dynamics calculation were performed with the SANDER module in AMBER9 [16]. Accurate force fields are essential for reproducing the conformational and dynamic behavior of the systems, the leaprc.ff99 [17] force fields are well parameterized for proteins but the parameters for small molecules are still limited. Accordingly, leaprc.glycam04 [18] was used for the carbohydrate molecule. A cutoff of 10 Å was applied to nonbonded interactions during all simulations.

The potential energy of the molecule was minimized in a three-stage energy minimization process [19]. First of all, 4000 steps of minimization were performed while keeping the solute atoms frozen with strong harmonic restraints. Secondly, 6000 steps of minimization were performed while keeping heavy atoms only in backbone restrained with a force constant 0.5 kcal mol^{-1} $Å^{-1}$ so that more flexibility was introduced into the side-chain conformations. Then, a third stage minimization of 20,000 steps was performed with all atoms relaxed.

The molecular dynamics simulations were performed with a starting temperature of 0 K followed by slowly heating to 300 K over the course of 40 ps, then it was allowed to stabilize for another 40 ps. After these equilibration stages, MD simulations were carried out for 2 ns including 1,000,000 cycles. The integration time step of 2 fs was employed in the simulations. All chemical bonds were constrained using the SHAKE algorithm [20]. During the full simulation, the system was maintained at the room temperature (300 K) and atmospheric pressure (101,325 Pa).

The MD simulation analysis was mainly performed with the PTRAJ module of the Amber9 program. Visualization and manipulation of the conformations was performed using the program VMD 1.8.6 [21] and Swiss-PdbViewer 3.7 [22].

MM-PBSA calculation

The free energy was calculated using the molecular mechanics Poisson–Boltzmann surface area (MM-PBSA) [23]. This is because the MM_PBSA approach combines

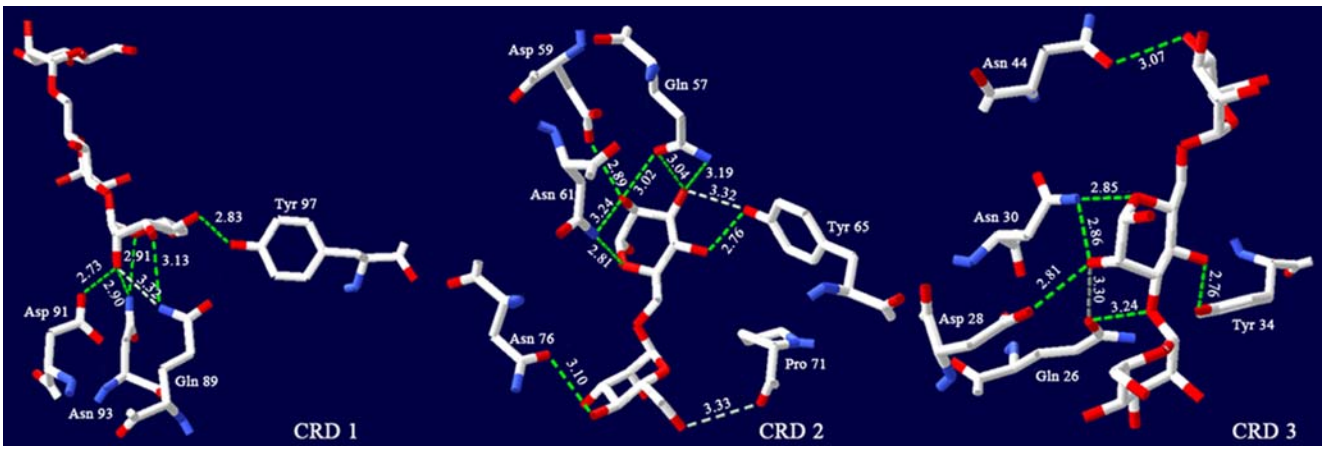

Fig. 4 Schematic illustrations of the hydrogen bond between GNA and the mannoside in the x-ray structure. Dashed lines indicate hydrogen bonds and its distance are labeled in angstroms (Å). Amino acid residues are labeled by three letter code

Table 1 Hydrogen bonds between GNA and the mannoside ligand at CRD1 in our MD simulation

Donor	AcceptorH	Distance (Å)	X-ray structure*
109 O3	Arg101 HE	3.085	no
109 O4	Arg101 HE	3.127	no
110 O2	Asn93 HD22	2.98	yes
110 O2	Gln89 HE21	3.029	yes
110 O3	Gln89 HE21	3.029	yes
110 O3	Asn93 HD22	3.111	yes
110 O4	Gln89 HE22	3.005	yes
110 O4	Tyr97 HH	3.01	yes
110 O5	Asn93 HD22	3.285	yes

* "yes" represent that hydrogen bonds exist in the x-ray structure while "no" means non-existent

the molecular mechanical energies with the continuum solvent approaches and it calculates the free energies of the end states directly, avoiding the time-consuming simulation of intermediate states. The explicit water molecules were removed from the snapshots.

The binding free energy ΔG_{bind} was estimated as follows:

$$\Delta G_{bind} = \Delta E_{gas} + \Delta G_{solv} - T\Delta S_{conf} \quad (1)$$

Where ΔE_{gas} is the interaction energy between the GNA and its mannoside ligand in the gas phase and is given by:

$$\Delta E_{gas} = \Delta E_{elec} + \Delta E_{vdw} \quad (2)$$

While ΔE_{elec} and ΔE_{vdw} represent the receptor-ligand electrostatic and van der Waals interactions, respectively.

Table 2 Hydrogen bonds between GNA and the mannoside ligand at CRD2 in our MD simulation

Donor	AcceptorH	Distance (Å)	X-ray structure*
112 O2	Asn76 HD21	3.069	yes
112 O3	Asn61 HD21	3.098	yes
112 O3	Gln57 HE21	2.949	yes
112 O4	Asn61 HD21	3.21	yes
112 O5	Asn76 HD22	3.047	yes
112 O6	Asn76 HD22	3.027	yes
112 O6	Gln80 HE22	3.011	no
112 O6	Asn61 HD21	3.014	yes
113 O2	Trp73 HE1	3.053	no
113 O4	Asn76 HD21	3.03	yes
113 O4	Trp73 HE1	3.03	no
113 O5	Trp73 HE1	3.133	no
113 O6	Trp73 HE1	3.014	no

* "yes" represent that hydrogen bonds exist in the x-ray structure while "no" means non-existent

The solvation free energy (ΔG_{solv}) was estimated as the sum of electrostatic solvation free energy (ΔG_{PB}) [24] and apolar solvation free energy (ΔG_{NP}):

$$\Delta G_{solv} = \Delta G_{PB} + \Delta G_{NP} \quad (3)$$

Solute entropies ($T\Delta S_{conf}$) were estimated by the NMODE module in AMBER 9 program.

Results and discussion

Protein structural features

To assess the stability of the GNA structures during the MD simulations, the root-mean square deviation (*RMSD*) values with respect to the initial structures were calculated along the 2 ns trajectories and shown in Fig. 2(a). Analyses of the figure indicate that the *RMSD* of both systems reaches an equilibration and oscillate around an average value after about 200 ps simulation time. And we found that the *RMSD* of both systems little increasing during the simulation run, these results indicate that both systems are stable on the whole, and their conformation changes to some extent. By comparing the *RMSD* of the complexed (with ligand) and uncomplexed (without ligand) systems, it was noted that there were no significant differences between the two systems. Although in the case of the uncomplexed structure, the *RMSD* was a little higher than the complexed structure, while with regard to a system of 108 residues, this slight fluctuation is negligible.

The total energy of the system is also essential to the stability of the system, and only the simulation of an energy

Table 3 Hydrogen bonds between GNA and the mannoside ligand at CRD3 in our MD simulation

Donor	AcceptorH	Distance (Å)	X-ray structure*
114 O2	Asn30 HD22	2.987	yes
114 O4	Asn30 HD22	2.965	yes
114 O5	Asn30 HD22	3.049	yes
114 O6	Asn30 HD22	3.026	yes
115 O2	Lys38 HZ3	2.954	no
115 O2	Tyr34 HH	2.955	yes
115 O4	Lys38 HZ2	2.917	no
115 O5	Lys38 HZ1	3.089	no
115 O6	Lys38 HZ2	2.959	no
116 O4	Asn44 HD22	2.991	yes
116 O6	Asn44 HD22	3.098	yes

* "yes" represent that hydrogen bonds exist in the x-ray structure while "no" means non-existent

Table 4 Difference of the hydrogen bond region between our MD simulation and the x-ray structure

	CRD1/ Residues	CRD2 / Residues	CRD3/ Residues
X-ray structure	89–97	57–76	26–44
MD simulation	89–101	57–80	30–44

stable system can make sense. Here, the total energy fluctuations of GNA with (black) and without (red) ligand versus simulation time are displayed in Fig. 2(b). It shows that the systems maintain the equilibration during the 2 ns simulation period. These data are in agreement with *RMSD*. The mean value of the complexed system is −51.24 kcal mol^{-1}, and with the ligand binding, the total energy of the system reduces to −61.93 kcal mol^{-1}. These mean that the GNA with ligand is in a more stable state than that without the ligand.

The examination of the two systems shows that the structure of GNA is stable with or without mannose. The binding of the ligand does not generate large modifications to GNA conformation, but it rather induces energy reduction to the system.

Secondary structure

In order to obtain a more detailed description of the flexibility of the structures, the secondary structure was calculated over the 2 ns trajectories and shown in Fig. 3. It shows clearly that both the ligand-bound and ligand-free conformations remain rather stable during 2 ns MD simulations (notice the continuity of the colored strips) although local conformational shape change is observed. In the region of residues 26–31, a disruption of the turn is observed in ligand-bound system during 260–540 ps; Residues 57–62, the two systems show the similarities of most time involved in irregular coils or beta-sheet or turns, and keep changing. Residues 88–95, the ligand-bound system has much more coils element but less turn element than the ligand-free system. According to Wright [5], the monomer of GNA contains three carbohydrate recognition domains (CRD), CRD1correspond to residues 89–97, CRD2 to residues 57–76 and CRD3 mainly to residues 26–34 (and Asn44), just similar to these high fluctuation regions. Therefore, these results indicate that conformational changes are mainly caused by ligand binding.

Furthermore, interesting mobility was observed around residue 20, that there was a noticeable loss of turn content in the ligand-bound system before 1000 ps. Also of interest in ligand-bound system was that the coil region between residues 102 and 107 changes to helix after 500 ps.

Hydrogen-bond analysis

Hydrogen bond is one of the main forces to maintain the binding of ligand and acceptor. Here, we proposed that a donor and an acceptor atom form a hydrogen bond when the distance between them is less than 3.5 Å and the H–O–H angle larger than 120°. The crystallographic data are displayed in Fig. 4 [5] and the MD simulation results are listed in Tables 1, 2 and 3. In general, our MD simulation reproduces most of the H-bonds present in the x-ray structure, or, they are in qualitative agreement. Although some of these hydrogen bond interactions are weak they make the complex more stable than the ligand-free conformation.

From Fig. 4, we know that the residues of Asp91 in CRD1 and Asp59 Tyr65 Pro71 in CRD2 as well as Asp28 Gln26 in CRD3 are involved in the hydrogen bond formation, however, no direct interaction was observed during the simulation. Additionally, some of the other important hydrogen bonds, not observed by crystallography, are established in the simulation (Tables 1, 2, and 3). However, results of the MD simulation hydrogen bond region agreed fairly well with x-ray experiments (Table 4). These discrepancies between the crystallographic data and our calculations might lie in that the crystallographic hydrogen bonds are listed regardless of the dynamic characters.

MM-PBSA

The MM-PBSA analysis allows us to separate the total free energy of binding into electrostatic, van der Waals interactions and solute-solvent interactions, and thereby

Table 5 Binding free energies (kcal mol^{-1}) resulting from MM/PBSA analysis of the GNA-mannoside complexes

ΔE_{elec}	ΔE_{vdw}	ΔE_{PB}	ΔG_{NP}	$T\Delta S$	Apolar/ hydrophobic	Polar/ electrostatic	ΔG_{bind}
−119.16	−42.49	26.50	−6.17	−52.66	−48.66	−92.66	−88.66

Apolar contribution = $\Delta E_{vdw} + \Delta G_{NP}$; Polar contribution = $\Delta E_{elec} + \Delta E_{PB}$

gain additional insights into the physics of the receptor-ligand association process. As shown in Table 5, electrostatic interaction plays a very important role in the simulation, contributing significantly more to the total interaction energy than the van der Waals interactions. Their values are −119.16 kcal mol^{-1} and −42.49 kcal mol^{-1}, respectively. Note that the internal component of the molecular-mechanical energy (bond, angle, and torsional energies) has zero contribution to the binding free energy, because the structures of GNA in its unbound and bound states were assumed to be the same (data not shown in the table).

Table 5 also reports the contributions of apolar/hydrophobic and polar/electrostatic to the free energy. We found that the predicted binding free energy is dominated by the magnitudes of the polar components ($\Delta E_{elecs} + \Delta E_{PB}$). In contrast, the apolar interactions ($\Delta E_{vdw} + \Delta G_{NP}$) shows less contribution to the binding free energy.

Conclusions

Galanthus nivalis agglutinin (GNA), which represents the super family of monocot mannose-specific lectins, has received much attention for its remarkable anti-HIV activities. In this work, we report 2 ns MD simulations of GNA in the presence and absence of the ligand. Our findings suggest that the binding of ligand did not alter the GNA structure to a significant extent but induce energy reduction to the system. The secondary structure dynamics reveal that the fluctuation occurs mainly in the carbohydrate binding region whereas other regions are rather stable. Over the period of the trajectory the hydrogen-bond analysis suggests that the interaction between GNA and its mannoside ligand is in qualitative agreement with the x-ray structure.

Accurate free energy estimation is needed in many predictive tasks such as structure-based drug design studies [25]. In the present study, the binding free energies were estimated using MM–PBSA method, and the results indicate that electrostatic interaction plays an important role in the simulation, about 76.67 kcal mol^{-1} more negative than the van der Waals interactions, and their binding affinities are determined by polar term rather than apolar/hydrophobic.

Previous studies showed that the envelope protein gp120 of HIV is highly glycosylated with mannose [8, 10–12]. While glycosylation of HIV gp120 provides a formidable barrier for development of strong antibody responses to the virus, it also provides a potential site of attack by the mannose binding lectin [9]. As mentioned above, our MD simulation results would provide a crucial clue for a better understanding of the carbohydrate binding mechanisms of GNA and the other monocot mannose-specific lectins. Furthermore, it may, therefore, provide more promising insights into pharmaceutical exploitation in treatment of HIV in the future.

Acknowledgments The authors acknowledge the UCSF (University of California, San Francisco) for providing us the AMBER 9 program package for free. We also thank Dr. Xiao Li for reading the manuscript and his useful suggestions.

References

1. Van Damme EJM, Peumans WJ, Barre A, Rouge P (1998) Plant lectins: a composite of several distinct families of structurally and evolutionary related proteins with diverse biological roles. Crit Rev Plant Sci 17:575–692
2. Van Damme EJM, Nakamura-Tsuruta S, Smith DF, Ongenaert M, Winter HC, Rouge P, Goldstein IJ, Mo H, Kominami J, Culerrier R, Barre A, Hirabayashi J, Peumans WJ (2007) Phylogenetic and specificity studies of two-domain GNA-related lectins: generation of multispecificity through domain duplication and divergent evolution. Biochem J 404:51–61
3. Van Damme EJ, Kaku H, Perini F, Goldstein IJ, Peeters B, Yagi F, Decock B, Peumans WJ (1991) Biosynthesis, primary structure and molecular cloning of snowdrop (Galanthus nivalis L) lectin. Eur J Biochem 202:23–30
4. Shibuya N, Goldstein IJ, van Damme EJ, Peumans WJ (1988) Binding properties of a mannose-specific lectin from the snowdrop (Galanthus nivalis) bulb. J Biol Chem 263:728–734
5. Wright CS, Hester G (1996) The 2.0 A structure of a cross-linked complex between snowdrop lectin and a branched mannopentaose: evidence for two unique binding modes. Structure 4:1339–1352
6. Hester G, Kaku H, Goldstein IJ, Wright CS (1995) Structure of mannose-specific snowdrop (Galanthus nivalis) lectin is representative of a new plant lectin family. Nat Struct Biol 2:472–479
7. Hester G, Wright CS (1996) The mannose-specific bulb lectin from Galanthus nivalis (snowdrop) binds mono- and dimannosides at distinct sites. Structure analysis of refined complexes at 2.3 Å and 3.0 Å resolution. J Mol Biol 262:516–531
8. Favero J (1994) Lectins in AIDS research. Glycobiology 4:387–396
9. Ji X, Gewurz H, Spear GT (2005) Mannose binding lectin (MBL) and HIV. Mol Immunol 42:145–152
10. Balzarini J, Schols D, Neyts J, van Damme EJ, Peumans W, de Clercq E (1991) Alpha-(1–3)- and alpha-(1–6)-D-mannose-specific plant lectins are markedly inhibitory to human immunodeficiency virus and cytomegalovirus infections in vitro. Antimicrob Agents Chemother 35:410–416
11. Leonard CK, Spellman MW, Riddle L, Harris RJ, Thomas JN, Gregory TJ (1990) Assignment of intrachain disulfide bonds and characterization of potential glycosylation sites of the type 1 recombinant human immunodeficiency virus envelope glycoprotein (gp120) expressed in Chinese hamster ovary cells. J Biol Chem 265:10373–10382
12. Hart ML, Saifuddin M, Uemura K, Bremer EG, Hooker B, Kawasaki T, Spear GT (2002) High mannose glycans and sialic

acid on gp120 regulate binding of mannose-binding lectin (MBL) to HIV type 1. AIDS Res Hum Retroviruses 18:1311–1317
13. Liu FF, Dong XY, Sun Y (2008) Molecular mechanism for the effects of trehalose on beta-hairpin folding revealed by molecular dynamics simulation. J Mol Graph Model 27:421–429
14. Kundu S, Roy D (2008) Temperature-induced unfolding pathway of a type III antifreeze protein: insight from molecular dynamics simulation. J Mol Graph Model 27:88–94
15. Jorgensen WL, C C, Madura JD (1983) Comparison of simple potential functions for simulating liquid water. J Chem Phys 79:926–935
16. Case DA, Cheatham TE 3rd, Darden T, Gohlke H, Luo R, Merz KM, Onufriev A, Simmerling C, Wang B, Woods RJ (2005) The Amber biomolecular simulation programs. J Comput Chem 26:1668–1688
17. Wang JM, Cieplak P, Kollman PA (2000) How well does a restrained electrostatic potential (RESP) model perform in calculating conformational energies of organic and biological molecules? J Comput Chem 21:1049–1074
18. Kirschner KN, Woods RJ (2001) Solvent interactions determine carbohydrate conformation. Proc Natl Acad Sci USA 98:10541–10545
19. AMBER online manual. http://ambermd.org/tutorials/advanced/tutorial8/loop2.htm
20. Larini L, Mannella R, Leporini D (2007) Langevin stabilization of molecular-dynamics simulations of polymers by means of quasisymplectic algorithms. J Chem Phys 126:104101
21. Humphrey W, Dalke A, Schulten K (1996) VMD: visual molecular dynamics. J Mol Graph 14:33–38
22. Guex N, Peitsch MC (1997) SWISS-MODEL and the Swiss-PdbViewer: an environment for comparative protein modeling. Electrophoresis 18:2714–2723
23. Kollman PA, Massova I, Reyes C, Kuhn B, Huo S, Chong L, Lee M, Lee T, Duan Y, Wang W, Donini O, Cieplak P, Srinivasan J, Case DA, Cheatham TE 3rd (2000) Calculating structures and free energies of complex molecules: combining molecular mechanics and continuum models. Acc Chem Res 33:889–897
24. Luo R, David L, Gilson MK (2002) Accelerated Poisson-Boltzmann calculations for static and dynamic systems. J Comput Chem 23:1244–1253
25. Li T, Froeyen M, Herdewijn P (2008) Computational alanine scanning and free energy decomposition for E. coli type I signal peptidase with lipopeptide inhibitor complex. J Mol Graph Model 26:813–823